# Chaotic scattering by steep repelling potentials

A. Rapoport* and V. Rom-Kedar†

*Faculty of Mathematics and Computer Science, The Weizmann Institute of Science, P.O. Box 26, Rehovot, Israel 76100*

(Received 21 May 2007; published 28 January 2008; publisher error corrected 29 January 2007)

Consider a classical two-dimensional scattering problem: a ray is scattered by a potential composed of several tall, repelling, steep mountains of arbitrary shape. We study when the traditional approximation of this nonlinear far-from-integrable problem by the corresponding simpler billiard problem, of scattering by hard-wall obstacles of similar shape, is justified. For one class of chaotic scatterers, named here regular Sinai scatterers, the scattering properties of the smooth system indeed limit to those of the billiards. For another class, the singular Sinai scatterers, these two scattering problems have essential differences: though the invariant set of such singular scatterers is hyperbolic (possibly with singularities), that of the smooth flow may have stable periodic orbits, even when the potential is arbitrarily steep. It follows that the fractal dimension of the scattering function of the smooth flow may be significantly altered by changing the ratio between the steepness parameter and a parameter which measures the billiards' deviation from a singular scatterer. Thus, even in this singular case, the billiard scattering problem is utilized as a skeleton for studying the properties of the smooth flow. Finally, we see that corners have nontrivial and significant impact on the scattering functions.

DOI: 10.1103/PhysRevE.77.016207 PACS number(s): 05.45.Df, 34.80.Bm, 72.10.−d

## I. INTRODUCTION

Since the days of Boltzmann, scientists have been using billiard models [1] to approximate the motion in systems with steep potentials; such models were used for studying various atomic and molecular dynamics problems [2–4], fragmentation phenomena in chemical reactions [5], various limits of the motion of point charges with Coulomb potentials (see [6–8] and references therein), cold atom's motion in dark optical traps [9], and microwave dynamics in cavities with soft walls [10]. Mathematically, one may formulate this approach by introducing a one parameter family of steep smooth potentials depending on a steepness parameter $\varepsilon$, and study the flows induced by the corresponding Hamiltonians in the domain $\mathcal{D}$ as follows:

$$H = \sum_{i=1}^{N} \frac{p_i^2}{2} + W(q;\varepsilon),$$
$$W(q;\varepsilon) \underset{\varepsilon\to 0}{\to} \begin{cases} 0 & q \in \mathcal{D}\setminus\partial\mathcal{D} \\ c & q \in \partial\mathcal{D} \end{cases}, \quad \mathcal{D} \subset \mathbb{R}^N. \tag{1}$$

This formulation allows one to examine whether, for sufficiently small $\varepsilon$, the simplifying approximation of the smooth flow by a billiard flow is justified. In the last decade, together with Turaev, we developed a *new perturbational approach* to the analysis of far from integrable $N$ degrees of freedom Hamiltonian systems of the form (1) by utilizing the singular billiard limit [11–16]. These works include two complimentary types of results: the first kind are persistence theorems—it is established that under some natural conditions on $W$ and $\mathcal{D}$, regular hyperbolic orbits of the limiting billiards are inherited by the smooth flow, and error estimates and next order corrections are derived [12]. The second type demonstrate that singular semiorbits of the billiards may give rise to stable motion in the steep smooth system. These results imply that the softness of the walls may destroy the ergodicity and the mixing properties of Sinai billiards (for compact $\mathcal{D}$) even when the walls are repelling, arbitrarily steep and the billiard is of arbitrarily high dimension [13–16] (see [9] for an experimental realization of this phenomenon). Notice that even in this singular case the billiard limit is utilized—it serves as a mathematical tool for establishing the emergence of stable motion in the smooth system. The focus in all these studies was on the compact $\mathcal{D}$ case. Here, we examine the implications and extensions of this theory and approach to the problem of chaotic scattering (noncompact $\mathcal{D}$) in two-dimensional geometries.

When a ray of inertial trajectories, parametrized by an input parameter, enters an interaction region in which the trajectories are modified by nonlinear forces, the ray is scattered and leaves the region in various directions. The observed *escape angles* and *residence times* are traditionally called *scattering functions* of the input parameter. Scattering problems arise in a wide spectrum of models in physics and chemistry (see [17] and [18]): celestial mechanics [19–24], charged particle trajectories in electric and magnetic field [25,26], hydrodynamical processes [27–31], models of chemical reactions [5,32–34] and scattering in atomic and nuclear physics [35,36]. Typically, most of the trajectories of the impinging ray stay in the interaction region for a finite time. However, in the Hamiltonian case, there may exist a Lebesgue-measure-zero set of input parameters producing trajectories that get trapped in the interaction region for an arbitrarily long time. This measure-zero set gives rise to strong oscillations in the scattering functions, influencing the nearby trajectories. When the invariant set associated with the scatterers has chaotic components, the singularity set of the scattering functions, which includes all initial conditions in the ray that belong to the stable manifold of the chaotic invariant set, is fractal [37,38]. Thus, traditionally, if for some ray the fractal dimension of the scattering function $d_\Phi$

*anna.rapoport@weizmann.ac.il
†vered.rom-kedar@weizmann.ac.il;
URL: http://www.wisdom.weizmann.ac.il/~vered

 

is larger than one [39] then the scattering is called chaotic [40], otherwise, it is called regular.

The structure of the scattering function was examined in diverse scattering problems. Hard-wall scatterers were studied in several two-dimensional geometries (three hard disks scatterers [37,5], three hard disks and a uniform magnetic field [25], billiard traps with two openings [41,42], disk moving along a Keplerian orbit [19,22], and a wedged billiard with gravity [20,43]). In some of these studies the dynamics on the invariant set is fully characterized by symbolic dynamics. Then, particle escape rates and other scattering characteristics may be found using the thermodynamic formalism [44,5]. In [45,46,25,47,48,38,7,8,49,17,50] scattering by finite range axis-symmetric potential hills and by smooth potential hills were studied. We note that at high energies, these scattering problems that arise in various fields of physics, may be formulated as scattering by steep repelling [51] potentials of the form (2) (scattering by smooth attractive potential wells [52,53] may require other analytical methodologies; see, e.g., [7,8,49]).

Due to the abundance of local and global bifurcations in nonintegrable systems, the structure of the invariant sets of scattering by smooth potential problems may depend sensitively on the energy and on the systems's parameters [45–47,54,32,55]. For example, the abrupt bifurcation, by which lowering the energy below a critical energy value $E_c$ leads to a sudden change in the topology of the Hill's region (the region of allowed motion in the configuration space [56]), creates a new hyperbolic invariant set which is structurally stable [57] and leads to *fully developed chaotic scattering* [45,46,58]. On the other hand, the appearance of islands of stability via local bifurcations [45,47,55], or the appearance of parabolic orbits (even without stability islands) [54], gives rise to nonhyperbolic scattering—the scattering functions appear to have singularities on a set of fractal measure one and thus $d_\Phi$ approaches two.

Summarizing, the following classification of typical scattering problems emerges; when the invariant set is simple (consists of a countable number of unstable periodic orbits) *regular* scattering is produced and $d_\Phi$ is one. When the invariant set is uniformly hyperbolic and has, on some appropriately defined section, a fractal dimension larger than one, *hyperbolic chaotic* scattering is created and $d_\Phi \in (1,2)$. Finally, when the invariant set is *nonhyperbolic* (containing KAM-tori or parabolic orbits), *nonhyperbolic chaotic* scattering is observed and $d_\Phi$ approaches 2. While for many billiard problems and finite range potentials the invariant set may be explicitly constructed by geometrical means, for the smooth case its structure is complex and is usually found via numerical simulations.

Here, we extend the methodologies of [11–16] to study scattering by a family of billiardlike potentials $W(q;\varepsilon)$, which, in the limit $\varepsilon \to 0$, becomes the hard-wall billiard scatterer $D=\cup_{i=1}^{n} D_i$. The $D_i$'s are smooth obstacles (compact closed smooth domains of "height" $\mathcal{E}_i$, where $\mathcal{E}_i > 0$ and may be infinite), $n$ is finite, and the distance between the obstacles is bounded from above (yet they may overlap). Rewriting Eq. (1) by setting $\mathcal{D}=\mathbb{R}^2 \setminus D$, we thus consider

$$H = \frac{\|p\|^2}{2} + W(q;\varepsilon), \quad W(q;\varepsilon) \underset{\varepsilon \to 0}{\to} \begin{cases} 0 & q \in \mathbb{R}^2 \setminus D \\ \mathcal{E}_i & q \in \partial D_{\mathrm{i}} \end{cases}, \qquad h \in (0, \mathcal{E} = \min_{\mathrm{i}} \mathcal{E}_i). \tag{2}$$

For example, the potential may be of a power-law form $W(q;\varepsilon)=\Sigma_{i=1}^{n} \varepsilon E_i / Q_i(q)$ or of exponential form $W(q;\varepsilon) = \Sigma_{i=1}^{n} E_i \exp[-Q_i(q)/\varepsilon]$, where $Q_i(q)$ is the distance from $\partial D_i$ [so $Q_i(q)|_{q \in \mathbb{R}^2 \setminus D_i} > 0$ and $Q_i(q)|_{q \in \partial D_i} = 0$]. More generally, $W(q;\varepsilon)$ may have local minima (yet their depth [59] must go to zero with $\varepsilon$), and point charges may be similarly studied (by considering a fictitious finite size obstacle with energy-dependent radii, see [6]).

At a fixed energy level below $\mathcal{E}$, for sufficiently small $\varepsilon$ values, the particle moves essentially freely between the obstacles and bounces of their boundary when it encounters them. Intuitively, one would expect that this motion is close to the scattering by the hard-wall scatterer $D$—this is the underlying hypothesis which made the hard-wall scattering models so popular. Formulating the scattering problem appropriately as a return map to some large circle $S_R^-$ which encloses $D$ (see Sec. II) and using the persistence results for regular hyperbolic orbits in $S_R^-$ [12], we establish here that for some scatterers—the regular Sinai scatterers—this intuitive result may be rigorously justified: their hyperbolic invariant sets are topologically conjugate (Theorem 1) and hence their scattering functions are similar (see Sec. III B).

Yet, we know that for the general steep repelling potential problem (1), singularities of the billiards (tangent orbits and semiorbits ending up in corners of the billiard domain) lead to substantial differences between the smooth flow and its billiard limit for arbitrary small $\varepsilon$ values [11–16]. Here, we explore the implication of this observation on the scattering problem. We are thus led to the study of the billiard singularities in this scattering context.

While the influence of tangent singularities on the invariant set of scattering systems was studied in [37,5,50], corner singularities (that arise only when the scatterers boundary is not smooth) have been mostly neglected (though see [20,43]). We propose that the appearance of corners affects the scattering in a nontrivial fashion even in the billiard case (see Sec. II E 2). Moreover, we expect these effects (and their smoothed counterparts) to be of physical significance in applications with nontrivial geometries such as scattering by complex molecules (we envision that the scatterers level sets are then composed of several convex, overlapping obstacles' hills, and the concave smooth meeting segments of these convex parts play the role of smoothed out corners). For such systems we show that the billiard-with-corners limit provides a useful skeleton for predicting the scattering by the smooth potentials (even though it is of an essentially different nature).

The paper is ordered as follows: in Sec. II we present a proper setup for the billiard scattering problem: we define the scattering map and the regular and singular Sinai scatterers, and explain how tangencies and corners influence their invariant set and their scattering functions. To demonstrate these effects we introduce two families of singular Sinai bil-

liard scatterers—one with smooth boundaries and the other with corners. In Sec. III a paradigm for studying chaotic scattering by smooth steep billiardlike potentials is presented. Indeed, once the scattering map is properly defined, the application of [11–16] to the scattering problem produces immediately nontrivial results regarding the structure of the invariant sets of smooth potentials limiting to hard-wall scatterers. In particular, we conclude that for regular Sinai scatterers the steep smooth flow and the limiting billiard scatterer have similar chaotic scattering functions. In Sec. IV, the scattering by steep smooth potentials is investigated when the limiting billiards are singular, having either a corner polygon or a tangent periodic orbit. It is demonstrated that the billiard singularities may be utilized to control the fractal dimension of the scattering functions of the steep smooth potentials. In the Appendix we include precise statements regarding the classes of potentials we consider and the rigorous persistence results that apply to these.

## II. BILLIARD SCATTERING

### A. Formulation

We first provide a formal definition of the scattering map so that standard tools regarding compositions of maps and the methodologies developed in [11–16] may be easily applied to the scattering problem. Consider a scattering billiard in $\mathbb{R}^2$; let $S_{\bar{R}}\subset\mathbb{R}^2$ denote a circle, centered at the origin, of finite radius $\bar{R}$, parametrized by $s\in[0,2\pi)$. The scatterer $D$, a collection of hard wall obstacles, resides inside $S_{\bar{R}}$. The obstacles are assumed to have piecewise smooth, $C^{r+1}$ components ($r>3$). We call the scatterer $D$ a *Sinai scatterer* if its boundary is composed of a finite number $\bar{n}$ of $C^{r+1}$-smooth *scattering* components $\Gamma_i$ that are either bounded away from each other by some minimal distance or have pairwise intersections at angles that are bounded away from zero [60]. We denote by $\Gamma^*$ the corner set at which the scatterer boundary is not smooth. Some of our results apply to a general scatterer geometry, yet, we will mostly consider Sinai scatterers. We notice that Sinai scatterers are regularly used as models for various scattering processes (see [61], and references therein).

A typical trajectory enters $S_{\bar{R}}$ at some $s_{\text{in}}$ with velocity $(p_x,p_y)=\sqrt{2h}(\cos\varphi_{\text{in}},\sin\varphi_{\text{in}})$, moves freely under the billiard flow, reflecting elastically from the obstacles inside $S_{\bar{R}}$, until it exits $S_{\bar{R}}$ at time $t_{\text{out}}$ at some point $s_{\text{out}}$ with velocity in the direction $\varphi_{\text{out}}$. Thus, the $\bar{R}$-dependent scattering map $\mathcal{S}(\bar{R}):(s_{\text{in}},\varphi_{\text{in}})\to\left(s_{\text{out}},\varphi_{\text{out}},t_{\text{out}}=\frac{\mathcal{L}(\cdot;\bar{R})}{\sqrt{2h}}\right)$, where $\mathcal{L}(\cdot)$ denotes the length of the orbit, may be naturally defined. Instead of using the $\bar{R}$-dependent coordinates $s_{\text{in}},s_{\text{out}}$ it is traditional to define the transformation to the $\bar{R}$-independent impact parameters $b_{\text{in}}$ and $b_{\text{out}}$ as follows:

$$b_{\text{in}}=\bar{R}\sin(\varphi_{\text{in}}-s_{\text{in}}) \quad \text{and} \quad b_{\text{out}}=\bar{R}\sin(\varphi_{\text{out}}-s_{\text{out}}). \tag{3}$$

The scattering map may be thus written in terms of the impact coordinates. The scattering functions at $(b_{\text{in}},\varphi_{\text{in}})$ are defined as

$$(\Phi(b),T(b))=(\varphi_{\text{out}}(b_{\text{in}}+b,\varphi_{\text{in}}),t_{\text{out}}(b_{\text{in}}+b,\varphi_{\text{in}})),$$

$$b\in J(b_{\text{in}},\varphi_{\text{in}}), \tag{4}$$

where $J$, in the nontrivial [62] case, is a closed interval containing the origin such that for all $b\in J(b_{\text{in}},\varphi_{\text{in}})$ the scattering is nontrivial: the initial condition $(b_{\text{in}}+b,\varphi_{\text{in}})$ does hit the scatterer. Let $\mathcal{J}(b_{\text{in}},\varphi_{\text{in}})=\{(b,\varphi)\,|\,b=b_{\text{in}}+\bar{b},\bar{b}\in J(b_{\text{in}},\varphi_{\text{in}}),\varphi=\varphi_{\text{in}}\}$ denote the corresponding phase-space section, so $\Phi$ and $T$ are the first and third components of $\mathcal{S}(\bar{R})|_{\mathcal{J}(b_{\text{in}},\varphi_{\text{in}})}$. Let $B(\chi,\theta)$ denote the billiard map associated with the scatterers inside $S_{\bar{R}}$, where $\chi$ parameterizes the scatterers boundaries [63] and $\theta\in\left[-\frac{\pi}{2},\frac{\pi}{2}\right]$ is the incidence angle. For any regular nontrivial $(b_{\text{in}},\varphi_{\text{in}})$, we may write

$$(b_{\text{out}},\varphi_{\text{out}})=S_{\text{out}}\circ B_k\circ B_{k-1}\circ\cdots\circ B_1\circ S_{\text{in}}(b_{\text{in}},\varphi_{\text{in}};\bar{R}),$$

$$t_{\text{out}}=\frac{\mathcal{L}(b_{\text{in}},\varphi_{\text{in}};\bar{R})}{\sqrt{2h}}, \tag{5}$$

where $B_i=B(\chi_i,\theta_i)$ correspond to the interior billiard map $\circ$ denotes map composition, and whereas $S_{\text{in}}$ and $S_{\text{out}}$ correspond to the mapping from $S_{\bar{R}}$ to the first (last) reflection values $(\chi_1,\theta_1)$ and $(\chi_k,\theta_k)$, respectively. More generally, for any nontrivial $(b_{\text{in}},\varphi_{\text{in}})$ an interior orbit may be defined as follows:

$$\mathcal{O}(b_{\text{in}},\varphi_{\text{in}})=\{\chi_i,\theta_i\}_{i=1}^{k}. \tag{6}$$

When $k$ is finite and all the $k$ reflections are regular (so $\theta_i\neq\pm\frac{\pi}{2}$ and $\chi_i\notin\Xi_{\text{corner}}$, where $\Xi_{\text{corner}}$ denotes the values of $\chi$ at $\Gamma^*$, the corner set), $(b_{\text{in}},\varphi_{\text{in}})$ is a regular value. Then, the composition (5) results in a smooth $C^r$ mapping with a smooth dependence of the scattering time $t_{\text{out}}$ on initial conditions. Since for Sinai scatterers the set of initial conditions resulting in singular orbits is of measure zero, it follows that for Sinai scatterers, for almost all initial conditions, the map $S$ is a smooth ($C^r$) mapping. In principle, there are exactly two sources for nonsmooth behavior of $S$: interior singularities that are associated with singular reflections from the scatterers and trapping singularities associated with the divergence of the number of interior reflections $k$ (i.e., $k\to\infty$).

### B. Interior billiard singularities

For Sinai scatterers, the only interior singularities that may appear [64] are related to tangencies and to corners. Such singularities lead to nonsmooth behavior and discontinuities in the scattering functions as explained next.

#### 1. Tangencies

Assume the orbit $\mathcal{O}(b_{\text{in}},\varphi_{\text{in}})$ is tangent to one of the scatterers at some point $(\chi_t,\theta_t)$ (so $\theta_t\in\{-\frac{\pi}{2},\frac{\pi}{2}\}$), and contains no other singularities. Thus, $k$ is finite, and for all $i\neq t$ the reflections are regular. It follows that $(b_{\text{in}},\varphi_{\text{in}})$ belongs to a singularity line $\Sigma_{\text{tan}}$ of initial conditions $(b,\varphi)$ that have a tangency at the $t$ iterate near $(\chi_t,\theta_t)$. A small neighborhood of $\Sigma_{\text{tan}}$ is thus divided by $\Sigma_{\text{tan}}$ to two parts—on one side of

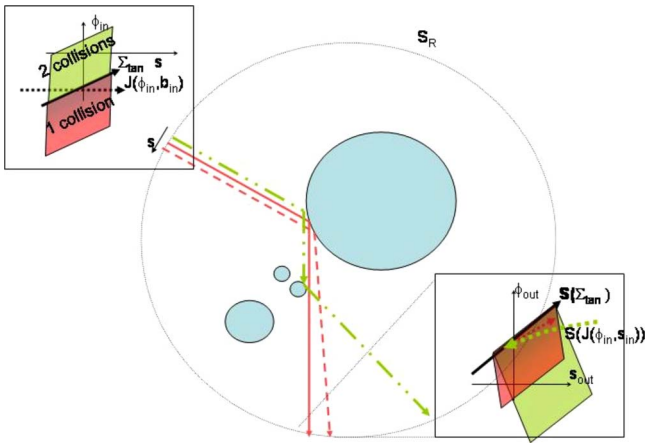


FIG. 1. (Color online) Scattering map and the effect of tangencies on it. Solid line—tangent orbit, dashed (dotted-dashed) line—a close-by orbit with initial condition below (respectively, above) $\Sigma_{\tan}$. The image of $J(b_{\text{in}},\varphi_{\text{in}})$ is not smooth and not monotonic across $\Sigma_{\tan}$.

$\Sigma_{\tan}$ trajectories reflect exactly $k$ times before escaping whereas on the other side trajectories have only $k-1$ reflections (see Fig. 1). Using the properties of the billiard map and flow near tangencies [65], it follows that the scattering map $S$ is $C^0$ [depends continuously yet not differentially on $(b,\varphi)$] across such singularity lines (see Fig. 1). Such tangent singularity lines may intersect—the transverse intersection point of two [66] such lines corresponds to orbits with two tangencies. Notice that for regular orbits of the Sinai scatterers the universal Sinai cone property holds—the cones $dq\cdot dp>0$ are forward invariant, and their orientation is preserved under an even number of reflections and reversed under an odd number of reflections. This property implies that at regular values $(b_{\text{in}},\varphi_{\text{in}})$, the function $\Phi(b;b_{\text{in}},\varphi_{\text{in}})$ is monotone whereas tangent values lead, in addition to the nonsmoothness, to nonmonotonicity (see Fig. 1).

#### 2. Corners

Assume the orbit $\mathcal{O}(b_{\text{in}},\varphi_{\text{in}})$ reaches a corner at its end point $(\chi_k,\theta_k)$, and contains no other singularities: $k$ is finite, $\chi_k\in\Xi_{\text{corner}}$, and for all $i<k$ the reflections are regular. Using the properties of the billiard map near regular corners (not cusps) [65], it follows that $(b_{\text{in}},\varphi_{\text{in}})$ belongs to a line $\Sigma_c$ of singular values of $(b,\varphi)$ all ending up at this corner point after $k$ reflections. Initial conditions starting arbitrarily close to $(b_{\text{in}},\varphi_{\text{in}})$ on one side of this singularity line hit first the upper boundary component near the corner, reflecting finally with some outgoing angle $\theta_k^+$ and initial condition on the other side first hit the lower boundary, reflecting finally with some outgoing angle $\theta_k^-$. Assume that the resulting two outgoing orbits escape to infinity after a finite number of regular reflections. Then, in general, all the components of the scattering map $S$ are discontinuous across $\Sigma_c$. Yet, $S$ is well defined and smooth on either side of this singularity curve (in particular, $t_{\text{out}}$ has a finite value for all initial conditions that do not belong to $\Sigma_c$). Other cases, for example, trapping of an outgoing trajectory by redirecting it into a corner (creating a corner polygon) or trapping by some components of the invariant set (creating a corner-hyperbolic invariant set—C-HIS—connection), are expected to appear at meeting points of $\Sigma_c$ with additional components of the singularity set. Listing all such generic constructions deserves a separate study. We denote by $\Sigma_{\text{bill}}=\Sigma_{\tan}\cup\Sigma_c$ the collection of singularity lines of initial conditions $(b_{\text{in}},\varphi_{\text{in}})$ that contain a billiard tangency or end up in a billiard corner.

### C. Trapping singularities

The singularities associated with the divergence of $k$ (i.e., when $k\to\infty$) are caused by orbits that asymptote the billiard's invariant set, its corner polygons or its C-HIS and HIS-C connections (it appears that only the first possibility was previously considered); denote by $\Lambda$ the generalized invariant set of $B$, which includes, in addition to the proper invariant set, all these singular semiorbits. Denote by $\Sigma_\Lambda$ the set of initial conditions $(b_{\text{in}},\varphi_{\text{in}})$ that never escape, so $k=\infty$ for these orbits and $S$ is not defined for them. The set $\Sigma_\Lambda$ contains all the initial conditions belonging to stable manifolds of the hyperbolic component of the invariant set $\Lambda_h$, and, if $\Lambda$ has nonhyperbolic components or includes singular semiorbits, it may contain other nonhyperbolic sticky orbits or orbits that asymptote singularities.

### D. Scattering functions and singularities for Sinai scatterers

Summarizing, let $\Sigma$ define the set of all singular initial conditions on $(b_{\text{in}},\varphi_{\text{in}})\in(-\bar{R},\bar{R})\times[0,2\pi):\Sigma=\Sigma_{\text{bill}}\cup\Sigma_\Lambda$. Then, for Sinai scatterers, the scattering functions $S$, $\Phi$, and $T$ are smooth and monotone away from the singularity lines composing $\Sigma$. Generically, these singularity lines cross the segment $\mathcal{J}(b_{\text{in}},\varphi_{\text{in}})$ transversely. In the simplest case $\Sigma_{\text{bill}}$ crosses $\mathcal{J}(b_{\text{in}},\varphi_{\text{in}})$ at isolated points [67] that correspond to simple tangent escaping orbits or to simple corner semiorbits. Across such isolated intersections of $\mathcal{J}(b_{\text{in}},\varphi_{\text{in}})$ with the singularity line $\Sigma_{\tan}$, $S$, $\Phi$, and $T$ are finite, continuous yet not smooth, and nonmonotone, see Fig. 3. In the corner case, i.e. across $\Sigma_c$, these functions are discontinuous, and, depending on the corner properties and on $\varphi_{\text{in}}$, may be monotone or nonmonotone (see [16] for the related analysis). Finally, near $\Sigma_\Lambda$ we will always have an accumulation of singularities. Near the intersection of $\mathcal{J}(b_{\text{in}},\varphi_{\text{in}})$ with the singularity lines corresponding to initial conditions belonging to the stable manifold of the hyperbolic component of $\Lambda$, $\Sigma_{\Lambda_h}$, the scattering functions have self similar structure and a diverging $T$. The behavior near other components of $\Sigma_\Lambda$ is yet to be studied (see, e.g., [55]).

### E. Regular and singular Sinai scatterers

We call the Sinai scatterer $D$ *regular* if it has no corners and its invariant set $\Lambda$ is bounded away from the singularity set so it is uniformly hyperbolic (the classical example of three identical circular scatterers of radius $a$ centered on the vertices of an equilateral triangle with edges of length $R$ is a regular Sinai scatterer for $R>3a$: then the invariant set $\Lambda_h$ is bounded away from any tangent trajectory, and $\Lambda_h$ is fully

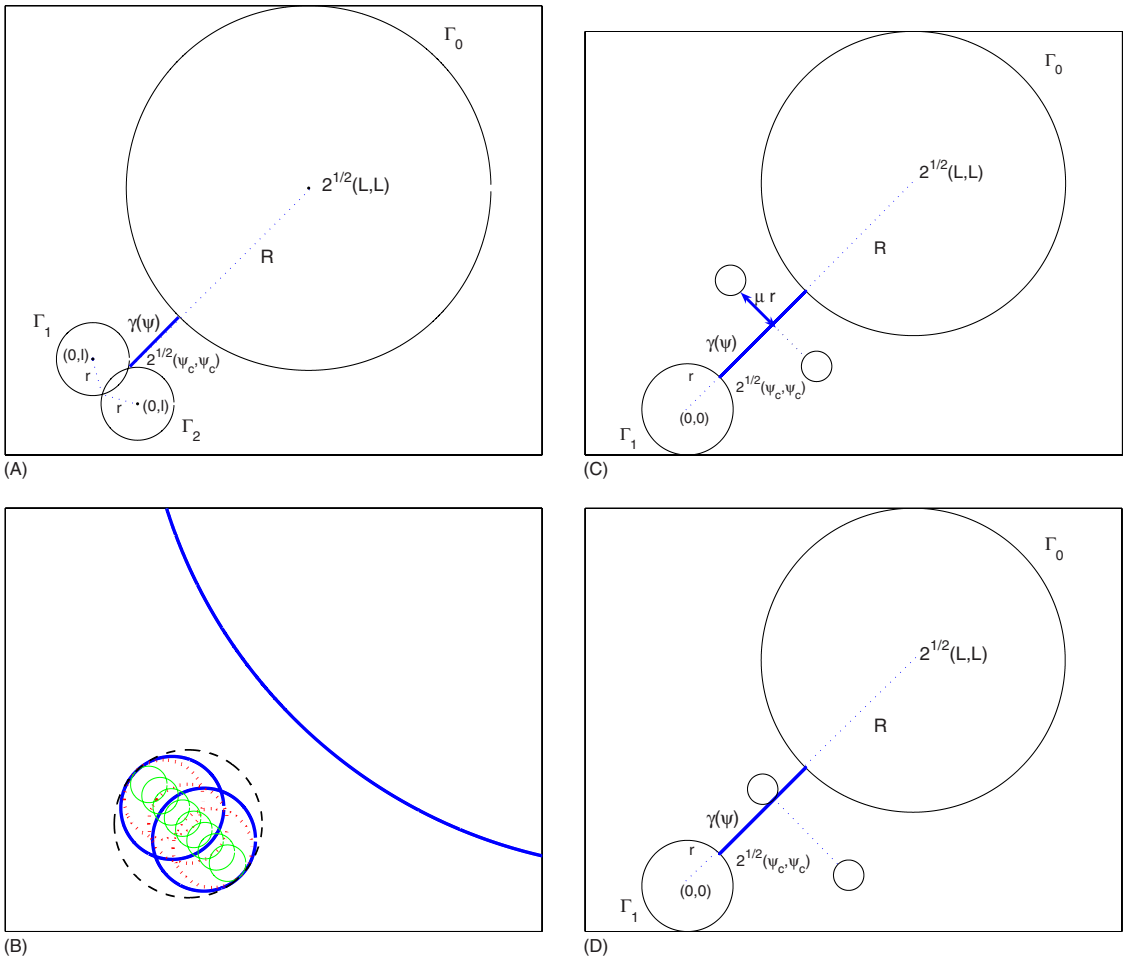


FIG. 2. (Color online) The geometries of the two singular Sinai scatterers. (A) The pearly billiard with one corner. (B) The pearly billiard with $n-1$ corners: dashed (black) $n=1$, bold (blue) $n=2$, dotted bold (red) $n=3$, solid (green) $n=8$. (C) The symmetric four-disks case ($\mu=K$). (D) The asymmetric tangent case: $\mu=0$.

described by symbolic dynamics on three symbols with a simple transition matrix [5]). In such a case, $\Lambda$ is structurally stable—a sufficiently small smooth deformation of $D$ does not change the symbolic dynamic description of the dynamics on $\Lambda$ nor its hyperbolic structure. The Sinai scatterer is *singular* when $\Lambda$ contains any singular orbits (tangent orbits) or singular semiorbits (corner polygons or C-HIS and HIS-C connections).

For regular Sinai scatterers, the hyperbolic structure of $\Lambda$ implies that for most $(b_{\text{in}},\varphi_{\text{in}})\in\Sigma_\Lambda$, the image under sufficiently many reflections of a small neighborhood of $\mathcal{J}(b_{\text{in}},\varphi_{\text{in}})$ aligns along the unstable manifold of $\Lambda$ and thus inherits its self-similar, fractal, and hyperbolic properties (see [37,5,17,50]).

When the invariant set $\Lambda$ undergoes a bifurcation, the Sinai scatterer becomes singular. For example, in the classical three identical disks scatterer problem, when the equidistance between the disks is decreased, orbits in $\Lambda$ undergo tangent bifurcations, a more detailed partition is needed, and the transition matrix becomes more complex, until, in the limit at which the disks touch each other (which is not a Sinai scatterer since cusps are created) infinite partition is achieved and the invariant set has a full measure [5]. Here, we choose two symmetric geometrical settings, inspired by [11,13,16], to examine such scatterers: the first corresponds to a billiard geometry with a tangency and the second to one with corners (see Fig. 2).

#### *1. Symmetric four disks scatterer—scatterers with tangent invariant orbits*

Consider four disks, $\Gamma_{0,1,2,3}$ of radii $R,r,r/2,r/2$, respectively, that are arranged as follows [see Figs. 2(C) and 2(D)]: $\Gamma_0$ is centered at $(x_0^c,y_0^c)=(\frac{L}{\sqrt{2}},\frac{L}{\sqrt{2}})$, $\Gamma_1$ at $(x_1^c,y_1^c)=(0,0)$, and $\Gamma_{2,3}$ are centers along the line $y=-x+1$ at a distance $2Kr$ apart, where the distance of $\Gamma_2$ from the diagonal is $\mu r$. At $\mu=0$ the diagonal is tangent to $\Gamma_2$, and at $\mu=K$ the circles $\Gamma_{2,3}$ are placed symmetrically with respect to the line $y=x$. The four-disk geometry corresponds to a regular Sinai billiard when the disks are placed sufficiently far from each other and sufficiently away from collinear configurations. At $\mu=0$ the invariant set has a tangent periodic orbit [Fig. 2(D)]. For most values of $\mu>0$ the invariant set is nonsingular, thus hyperbolic, producing a self-similar scattering function with fractal dimension greater than one, exactly as in [37,5,17,50]. To examine the behavior near a singular Sinai scatterer we fix $R=10r$, $L=13r$, $r=1$ and $\mu=K=0.1r$ so

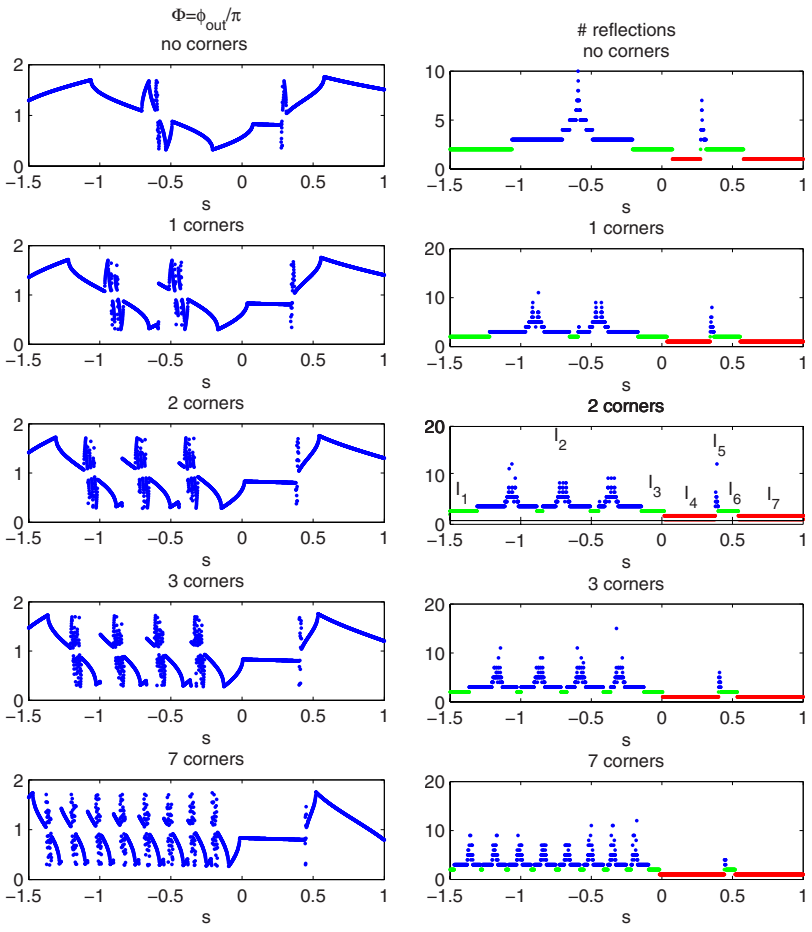


FIG. 3. (Color online) Scattering function for the $n$-pearls scatterer $\Phi_n(s)$ and the corresponding number of reflections $T_n(s)$ ($T=1$, red; $T=2$, green; $T\geq 2$ blue) for different values of $n$.

the diagonal belongs to the symmetry line of the scatterer and is close to being tangent.

#### 2. Pearly scatterer—scatterers with corners

Consider $n+1$ disks, $\Gamma_{0,1,\ldots,n}$ of radii $R, r_n, \ldots, r_n$, respectively, that are arranged as follows [see Figs. 2(A) and 2(B)]: $\Gamma_0$ is centered at $(x_0^c, y_0^c)=\left(\frac{L}{\sqrt{2}}, \frac{L}{\sqrt{2}}\right)$ and the disks $\Gamma_{1,\ldots,n}$ are centered along the line $y=-x+\frac{1}{\sqrt{2}}\left(\frac{\sqrt{1-\mu^2}}{\sqrt{1-\mu^2}+1}\right)$ so that they cover uniformly an interval of length $r$. The radius $r_n(\mu)$ is chosen so that for all $n$ the angle between [68] any two neighboring circles is $\alpha(\mu)$ as follows:

$$\alpha = \pi - \arccos[1-2(1-\mu^2)],$$

$$r_n = \frac{r}{2[1+(n-1)\sqrt{1-\mu^2}]}, \quad \mu \in [0,1]. \tag{7}$$

Hereafter we fix $R=10r$, $L=r(12+\mu+\sqrt{1-\mu^2})$, $r=1$ and vary $n$ and $\mu$. This geometry corresponds to a singular Sinai scatterer for any finite $n$ and $\mu \in (0,1)$. Following the same procedure as in [5], for most values of $\mu \in (0,1)$ one may fully characterize the invariant set using symbolic dynamics in which the $n+1$ symbols $\{0,1,\ldots,n\}$ encode the order of the collisions with the circles $\Gamma_i$, and, since the circles are dispersing, the sequence $\Gamma_i\Gamma_i$ is always forbidden. The detailed phase space partition and the corresponding transition matrix depend on $\mu$ in a nontrivial fashion; for $\mu$ values that are close to 1 we expect that the symbolic sequences in the invariant set will be simple and consist of pairs of collisions of the form $\Gamma_i\Gamma_0$ with $i\neq 0$ (for such $\mu$ values collisions between neighboring small circles $\Gamma_i\Gamma_{i\pm 1}$, with $i, i\pm 1\neq 0$, are subsequently reflected to infinity and do not belong to the invariant set). On the other hand, for small $\mu$'s, sequences of the form $\Gamma_i\Gamma_{i+1}\Gamma_i\cdots\Gamma_{i+1}\Gamma_0$ with preamble of varying length of up to $\left[\frac{\pi}{\alpha(\mu)}\right]$ collisions between the neighboring scatterers $\Gamma_i$ and $\Gamma_{i+1}$ are expected to emerge (in the non-Sinai limit of $\mu\to 0$ an infinite partition is needed). Thus, we expect that the fractal dimension of the scattering function will be increased as $\alpha(\mu)$ is decreased. The study of the topological changes of the invariant set as $\alpha(\mu)$ crosses the rational angles $\pi/m$ is interesting.

Figure 3 demonstrates some of these corner effects for $\mu=0.9$ and several $n$ values. It clearly shows that each additional corner leads to an additional unresolved region, a property that is kept under the self-similar magnification. It also demonstrates that the scattering functions are indeed *discontinuous* across $\Sigma_c$. To supply further details regarding the scattering of an incoming ray of initial conditions we divide this ray to resolved (trajectories escaping after one or two reflections) and unresolved (trajectories remaining close to the stable manifold of the unstable periodic orbits) intervals $I_j$, and describe their corresponding symbolic dynamics in Table I (see Figs. 3 and 4, left). On the resolved intervals $I_{1,3,4,6,7}$ the scattering function is smooth and monotone (see Figs. 3 and 4, left). The unresolved intervals $I_{2,5}^j$ may be

TABLE I. Resolved/unresolved intervals of the scattering function at $\mu=0.9$.

| Interval | $T$ | Collisions | Resolved/unresolved | Color |
|---|---|---|---|---|
| $I_1$ | 2 | $\Gamma_0\Gamma_n S_{\bar{R}}$ | R | Green |
| $I_2^j$ | $\geq 2$ | $\Gamma_0\Gamma_j\ldots$ $(j=1,\ldots,n)$ | U | Blue |
| $I_3$ | 2 | $\Gamma_0\Gamma_1 S_{\bar{R}}$ | R | Green |
| $I_4$ | 1 | $\Gamma_0 S_{\bar{R}}$ | R | Red |
| $I_5^j$ | $\geq 2$ | $\Gamma_n\Gamma_0\Gamma_j\ldots$ $(j=1,\ldots,n)$ | U | Blue |
| $I_6$ | 2 | $\Gamma_n\Gamma_0 S_{\bar{R}}$ | R | Green |
| $I_7$ | 1 | $\Gamma_n S_{\bar{R}}$ | R | Red |

further subdivided to $n$ unresolved regions according to their next collision, and this process can be further repeated in a self-similar manner, namely, we propose that for $\mu=0.9$ a fully chaotic scattering is developed for $n\geq 2$.

Since all the trapping trajectories at $\mu=0.9$ consist of pairs $\Gamma_0\Gamma_j$ (with $j\neq 0$), the magnification factor $M(n)$ of the corresponding self-similar invariant set depends linearly on the curvature of the small circles (7) [see the right part of Fig. 4, where, for $n\leq 10$ and a fixed $\mu=0.9$ we obtain $\ln(M(n);\mu=0.9)\approx 1.3+\ln(1/r_n)$]. Moreover, the growth factor in the number of unresolved intervals at this value of $\mu$ is observed to be $n$. Thus, the fractal (box-counting) dimension of the singularity set is estimated by

$$F(n;\mu=0.9)=\frac{\ln(n)}{\ln(M(n),0.9)}\approx\frac{\ln(n)}{1.3+\ln(1/r_n)},\qquad(8)$$

where $r_n$ is defined by Eq. (7). The dependence of this expression on $\mu$ and larger $n$ values is yet to be explored. From Eq. (7) we conjecture that this fractal dimension approaches 1 as $n$ is increased at a fixed $\mu$ value (a somewhat expected result—the boundary of the scatterer becomes nonsmooth in this limit).

Thus, we propose that there are *two mechanisms* to increase the complexity of the scattering functions in nontrivial billiard geometries with corners—one by increasing the number of corners and the other by making the corners sharper.

## III. SCATTERING BY STEEP POTENTIALS

### A. Formulation

Consider the smooth two-dimensional Hamiltonian flow (2) with the steep, billiardlike potential $W(q;\varepsilon)$, that limits, as $\varepsilon\to 0$, to the hard-wall scatterer problem in the closed region (with boundary) $\mathcal{D}=S_{\bar{R}+\Delta}^{\text{interior}}\backslash D$, where $\Delta>0$. Roughly, we require $W(q;\varepsilon)$ to asymptotically vanish away from the scatterer, we require that the level sets of $W(q;\varepsilon)$ approach smoothly the scatterer boundary, and that the normal force on these level sets is repelling so that the time spent near the scatterers' boundary is small and depends smoothly on the initial conditions. For example, potentials of the form $W(q;\varepsilon)=\Sigma_{i=1}^{n}E_iV_i\left(-\frac{Q_i(q)}{\varepsilon}\right)$, where $Q_i(q)|_{q\in\partial D_i}=0$, $Q_i(q)|_{q\in\mathcal{D}}>0$, $E_i\geq\mathcal{E}>0$, $N$ is finite, and there exists an $\alpha>0$ such that the smooth functions $V_i$ satisfy [69]

$$V_i(0)\geq 1,\quad V_i(z)>0,\quad V_i(z)=O_{C^{r+1}}\left(\frac{1}{z^\alpha}\right)\quad\text{for } z\gg 1,\qquad(9)$$

are billiardlike potentials. Conditions I–IV listed in the Appendix imply that for all $h\in(0,\mathcal{E}=\min_i E_iV(0))$ and sufficiently small $\varepsilon$ (nonuniformly in $h$), the Hill's region in $S_{\bar{R}}$ has the same topology as $\mathcal{D}$. Equivalently, let $W_{\max}(\varepsilon)$, $W_{\min}(\varepsilon)$, $W_{\text{sad}}(\varepsilon)$, and $W_{\max-\bar{R}}(\varepsilon)$ be the sets of the potential values at its local maxima, minima, and saddle points in $\mathcal{D}$, and its maximal value on $S_{\bar{R}}$, respectively. Notice that $\{W_{\max}(\varepsilon),W_{\min}(\varepsilon),W_{\text{sad}}(\varepsilon),W_{\max-\bar{R}}(\varepsilon)\}\to\{\{E_iV(0)\},0,0,0\}$ as $\varepsilon\to 0$, so, there exists $\varepsilon_{\max}(h)$ such that for any $\varepsilon\in(0,\varepsilon_{\max}(h))$, the local maxima values $\{W_{\max}(\varepsilon)\}$ are all larger than $h$ and all the other extremal points are below $h$: $\max\{W_{\min}(\varepsilon),W_{\text{sad}}(\varepsilon),W_{\max-R}(\varepsilon)\}<h<\min\{W_{\max}(\varepsilon)\}$, for all $\varepsilon\in(0,\varepsilon_{\max}(h))$. Thus, $\varepsilon_{\max}(h)$ serves as an upper bound for $\varepsilon$ values for which the current approach may be applicable [70]—for $\varepsilon>\varepsilon_{\max}(h)$ the topology of the Hill's region of the smooth flow is different than the topology of $\mathcal{D}$ (see Fig. 5).

Define the scattering map [71] of the smooth flow $S^\varepsilon(\bar{R})$ as the return map to the section $q\in S_{\bar{R}}^-:S^\varepsilon(\bar{R}):(s_{\text{in}},\varphi_{\text{in}})\to(s_{\text{out}}^\varepsilon,\varphi_{\text{out}}^\varepsilon,t_{\text{out}}^\varepsilon)$. Next, we examine the properties of $S^\varepsilon(\bar{R})$ for various types of scatterers.

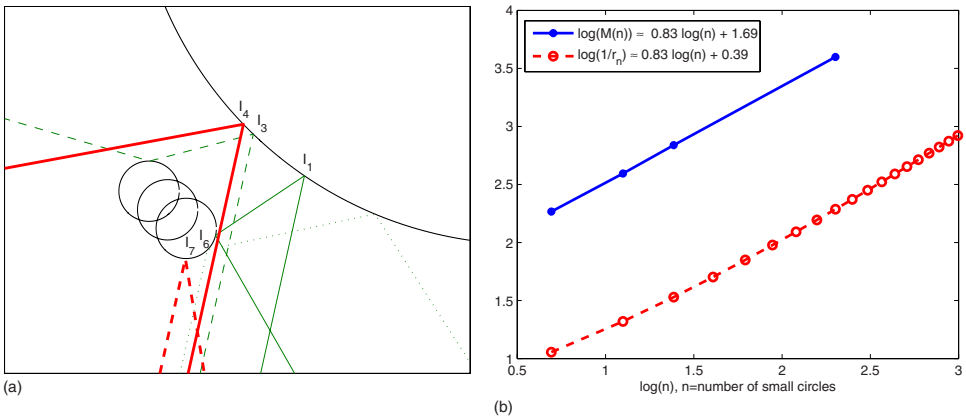


FIG. 4. (Color online) Left: The trajectories corresponding to the intervals of initial conditions $I_1$ (solid), $I_3$ (dashed), $I_4$ (bold), $I_6$ (dotted), and $I_7$ (bold dashed). Right: The magnification factor and the curvature of small disks as a function of $n$ in a natural logarithmic scale.

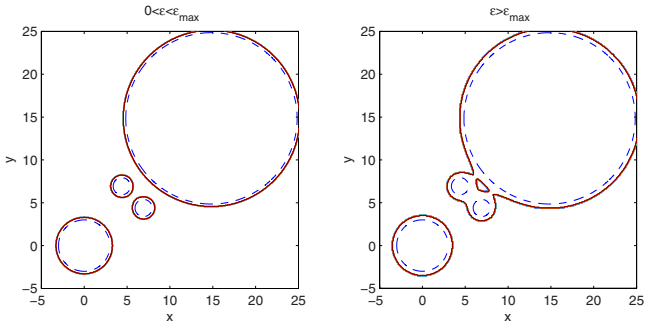


FIG. 5. (Color online) The level set of the exponential potential at $h=\frac{1}{2}$ for $\epsilon=0.3\in(0,\epsilon_{\max}(\frac{1}{2})=0.6)$ (left) and $\epsilon=0.75>\epsilon_{\max}$ (right). The dashed circles correspond to the billiard limit.

### B. Closeness theorems

Using the formulation developed in Sec. II in which the scattering map is appropriately defined, and the above definition of $\mathcal{D}$ and $S^{\varepsilon}(\bar{R})$, the methodologies developed in [12,14] may be now applied to the scattering problem. These imply, for example, that some orbits of $S(\bar{R})$ are shadowed by orbits of $S^{\varepsilon}(\bar{R})$: if $(s_{\rm in}(b_{\rm in},\varphi_{\rm in};\bar{R}),\varphi_{\rm in})$ is a nontrivial regular value (respectively, $(s_{\rm in},\varphi_{\rm in})\in\Sigma_{\tan}$ has a finite number of collisions, one tangent and all the rest regular) of the billiard scattering map $S$, then, there exists a nearby initial condition $(s_{\rm in}^{\varepsilon},\varphi_{\rm in}^{\varepsilon})$, limiting to $(s_{\rm in},\varphi_{\rm in})$ as $\varepsilon\to 0$, such that the smooth scattering map $S^{\varepsilon}$ is $C^r$ close [72] (respectively, is $C^0$ close) to $S$ at $(s_{\rm in},\varphi_{\rm in})$ (see the Appendix for details and error estimates). Most importantly, we can now establish that for regular Sinai scatterers the smooth flow and the billiard scatterer have the same scattering properties since their invariant sets are similar (see the Appendix).

*Theorem 1.* Consider the Hamiltonian system (2) with a billiardlike potential $W(q,\varepsilon)$ defined in the domain $\mathcal{D}=S^{\rm interior}_{\bar{R}+\Delta}\backslash D$, where $\Delta>0$, and $D$ is a *regular Sinai scatterer* so that $\Lambda$ is a nontrivial uniformly hyperbolic invariant set of $B$. Then, the energy level $h\in(0,\mathcal{E})$ contains, for sufficiently small $\varepsilon$, a uniformly hyperbolic invariant set $\Lambda^{\varepsilon}$, which is topologically conjugate to $\Lambda$. Moreover, the local stable and unstable manifolds of $\Lambda^{\varepsilon}$ are $C^r$ close to the local stable and unstable manifolds of $\Lambda$.

The self-similar structure and the fractal dimension of the scattering functions of the smooth flow thus limit to the corresponding structures of the billiard scatterers. These positive conclusions, which allow one to approximate smooth flows by billiards, are natural and are clearly observed in various simulations (e.g., Fig. 11). We do note though that without the correct setup of Sec. II and the machinery developed in [12,15] it is not obvious how to prove such results: the limit of the smooth flow to the billiard flow is singular (e.g., the vector fields associated with these two flows are not close even in the $C^1$ topology).

For example, to study the problem of scattering by $n$ centers of Coloumbic potentials (e.g., charged particles), a sophisticated and beautiful mathematical setup was developed to prove that in the high energy limit the invariant set is hyperbolic provided the centers are not collinear [7,8,49]. We propose that by introducing another fictitious radius parameter as in [6], the above corollary may be used to construct an additional proof of this result for the repelling case. Moreover, the current tools may be employed to detect configurations and (high) energy levels at which the invariant set in the repelling Coulombic case is nonhyperbolic.

In fact, Theorem 1 may be easily formulated in a more general form—for any two-dimensional scatterer geometry, for sufficiently small $\varepsilon$, any isolated component of the invariant set which is hyperbolic and is bounded away from any singularity of the billiard map—persists.

## IV. BILLIARD SINGULARITIES AND STEEP POTENTIAL SCATTERING

Since tangent and corner singularities of billiards' orbits may lead to stable orbits of the smooth flow [14–16], we expect that when $\Lambda$ has such singularities the smooth flow and the billiard will have a substantial different scattering function. To demonstrate these effects we consider two families of Hamiltonian flows that limit to the two geometrical settings introduced in Secs. II E 1 and II E 2 as follows:

$$H=\frac{p_x^2}{2}+\frac{p_y^2}{2}+W(x,y;\mu,\varepsilon), \tag{10}$$

where $\varepsilon$ controls the steepness of the potential and $\mu$ controls the billiard geometry: in the four-disk case $\mu$ controls the distance of the diagonal orbit from tangency, whereas for the pearly scatterers $\mu$ controls the angle between the neighboring small disks. The potential $W$ is a sum of exponentials as follows:

$$W_{\rm corner}(q;\varepsilon)=\exp\left(-\frac{Q_0(q)}{\varepsilon}\right)+\frac{1}{n}\sum_{k=1}^{n}\exp\left(-\frac{Q_k(q)}{\varepsilon}\right), \tag{11}$$

$$W_{\rm tangent}(q;\varepsilon)=\sum_{k=0}^{3}\exp\left(-\frac{Q_k(q)}{\varepsilon}\right), \tag{12}$$

where $Q_j(q)$ (the pattern function of [12]) is the distance between $q=(x,y)\in\mathcal{D}_{\rm Hill}(h,\mu,\varepsilon)$ and the disk $\Gamma_j$, where $\mathcal{D}_{\rm Hill}(h,\mu,\varepsilon)$ denotes Hill's region. We consider sufficiently small $\varepsilon$ values so that there are no abrupt bifurcations at $h=1/2$ [so the topology of $\mathcal{D}_{\rm Hill}(h,\mu,\varepsilon)$ is fixed (see Fig. 5)].

### A. Stable symmetric periodic orbit

The singular diagonal lines that correspond to singular orbits (semiorbits) of the asymmetric four disks (pearly) billiards, are expected to produce wedges of stability in the $(\mu,\varepsilon)$ plane [14–16]. These wedges emanate from isolated $(\mu^*,0)$ values, and the smooth flow has stable periodic orbits for all parameter values in these wedges. Figure 6 shows these wedges of stability for the one-corner case (found numerically, see [11] for methods). Observe that for a fixed $\mu$ there exist intervals of $\varepsilon$ values where the diagonal periodic orbit is elliptic: the real part of the two eigenvalues of the

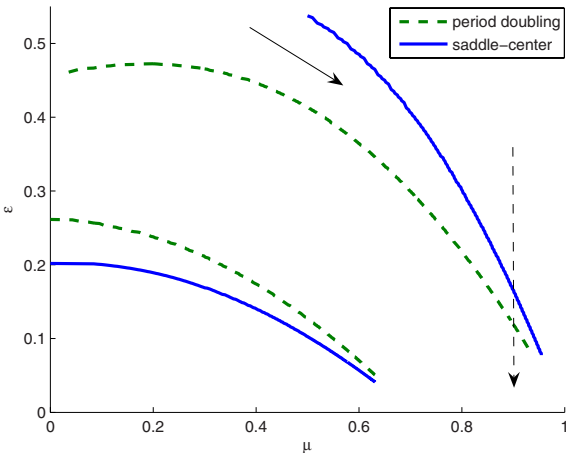


FIG. 6. (Color online) Wedges of stability of the diagonal orbit for the smooth one-corner case ($n=2$). The two shown wedges are bounded between the saddle-center bifurcation curve (solid line) and the period-doubling bifurcation curve (dashed line). The parameter values of Fig. 8 are taken along the dashed arrow line. The solid arrow indicates a possible choice of a curve $(\mu(\varepsilon),\varepsilon)$ along which stability islands exist for arbitrary small $\varepsilon$ values.

Poincaré map lie in the interval $[-1,1]$ [Figs. 7(A) and 8(A)]. In Figs. 7(B) and 8(B) we present phase portraits of the Poincaré return maps near the diagonal orbits for selected values of $\varepsilon$ (inside the stability wedges, close to their boundary and bounded away from them). The stability islands of these maps at $(\mu,\varepsilon)$ values in the wedges, the period-doubling bifurcations, and the hyperbolic escape from the vicinity of the diagonal for the unstable cases are clearly observed for both the tangent and corner geometry.

### B. Scattering by steep potentials near the billiard singularities

The scattering function dependence on $\varepsilon$ near a singular pearly Sinai scatterer ($n=2$ and $\mu=0.9$) is shown in Figs. 9–11.

(1) The billiard scattering at $\mu=0.9$ is chaotic and its invariant set appears to be uniformly hyperbolic [73] (Fig. 11, bottom): the regions that exhibit self-similar behavior are bounded away from the discontinuity point that is associated with the corner. Thus, the billiard scattering function exhibits the typical self-similar structure discussed in Sec. II E 2.

(2) At $\varepsilon=0.01$ the scattering function resembles the chaotic billiard scattering function and possesses the same type of self-similarity (Fig. 11, top). We propose that this observation is closely related to the generalization of Theorem 1: since the scattering near the invariant set is regular hyperbolic and $\varepsilon$ is sufficiently small the invariant set persists, and the self-similar structure of its local stable manifold persists as well. On the other hand, in theorem 1 corners were not allowed. Indeed, since the diagonal represents a possible mechanism for a recurrent motion near the corner (a valid corner polygon, see [16]), the invariant set of the smooth flow has this *additional new component*—the diagonal orbit, which, for this value of $\varepsilon$, is hyperbolic. We see that the scattering function of the smooth flow has an additional unresolved region of nonmonotonicity associated with this diagonal orbit, and thus, we expect that the smooth flow will develop some nonhyperbolic behavior near this region. Furthermore, interactions between the two components of the invariant set are expected to appear, as described next.

(3) At $\varepsilon=0.066\,54$ the nonmonotone behavior associated with the corner discontinuity appears to merge with the invariant set so one unresolved region disappears (Fig. 9).

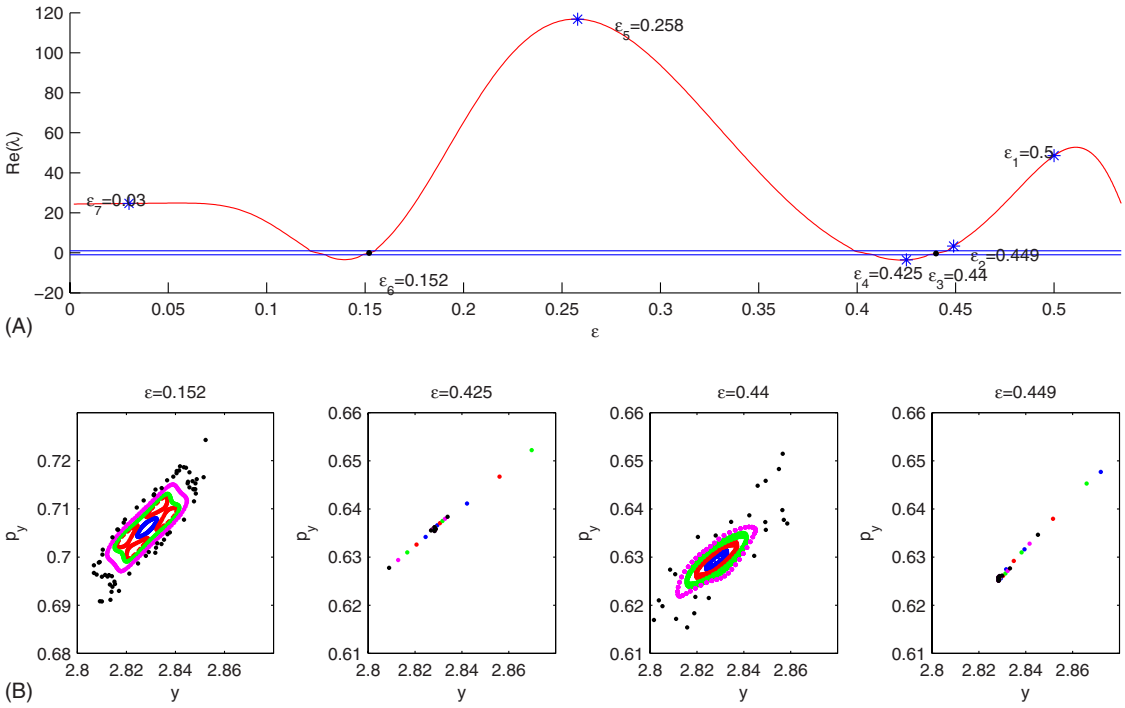


FIG. 7. (Color online) (A) The real part of $\lambda(\epsilon)$ for the tangent case at $\mu=K=0.1$. (B) The return maps near the diagonal to a section $(y,p_y)$ with a fixed $x$ and $p_x>0$ for selected $\epsilon$ values.

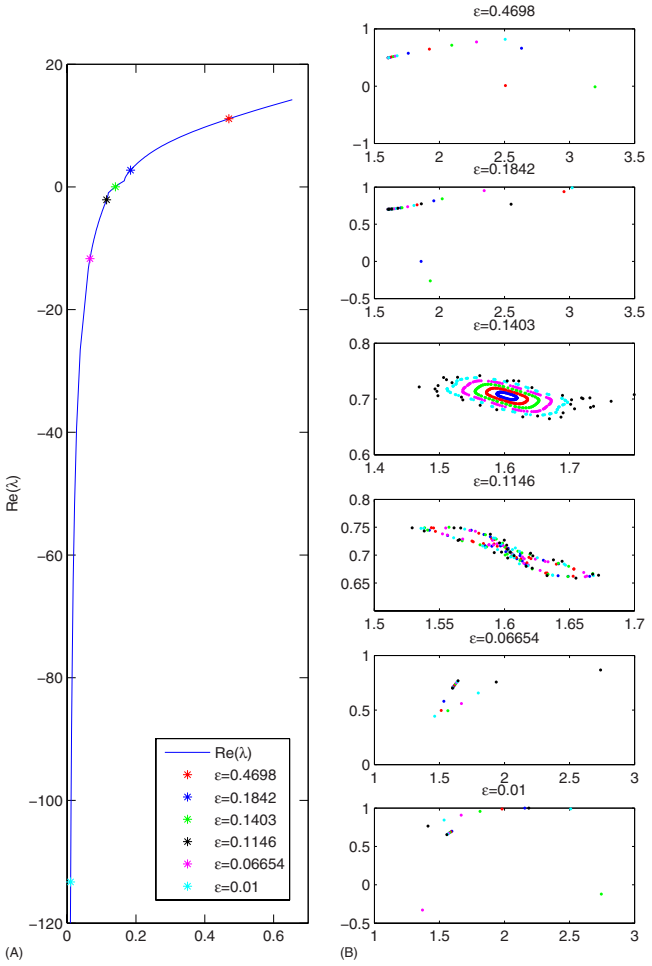


FIG. 8. (Color online) (A) The real part of λ for the corner case $n=2$, $\mu=0.9$. (B) The corresponding return maps for $\epsilon$ values shown in (A).

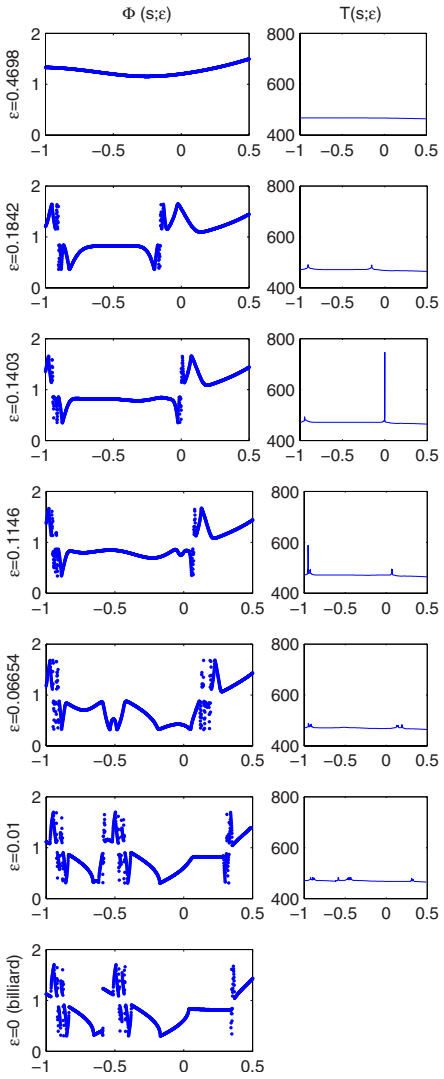


FIG. 9. (Color online) Scattering function $\Phi_2(s;\epsilon)$ and escape time $T_2(s;\epsilon)$ for the pearly case with $n=2$.

While self-similarity is still observed, its structure certainly appears to be different than the billiard scattering function. Here, we see that the bifurcations associated with the corner influence the structure of the invariant set.

(4) For $\varepsilon=0.1403$ (elliptic island) and $\varepsilon=0.1146$ (period doubling) the residence time functions $T(s;\varepsilon)$ have significant peaks (see Fig. 9) that are associated with sticky orbits. The scattering functions for these values of $\varepsilon$ appear to have a fractal dimension close to 2: at the center of Fig. 10 we show that zooming in the unresolved regions produces singular curves with widespread singularities. Both findings are typical to the scattering functions that appear when the invariant set has KAM tori [55].

(5) At $\varepsilon=0.1842$, above the wedge of stability, the scattering is regular as in scattering by two disks: the level sets near the corner are so smooth that the invariant set consists of only one hyperbolic periodic orbit.

(6) For $\varepsilon=0.4698$ the invariant set for the energy level $h=1/2$ is empty and the scattering function $\Phi(s;\varepsilon)$ is smooth.

A similar behavior is observed in the tangent geometry, as shown in Fig. 12; while increasing $\varepsilon$ leads to the merger of unresolved intervals, by zooming in on the chaotic zones it can be shown that the fractal dimension of the scattering function at the stability wedges appears to approach two.

## V. SUMMARY AND CONCLUSIONS

We propose that by utilizing the singular billiard limit, the structure of the scattering function of a class of smooth potentials—the billiardlike potentials—may be found. We demonstrated the feasibility and implications of this approach on a class of two-dimensional dispersing billiards—the regular and singular Sinai scatterers. For the regular scatterers we show that the scattering functions of the smooth flow limit to that of the billiards'. For the singular Sinai scatterers, we propose that the following scenario emerges: Let $\mu^*$ denote a bifurcation value for which the billiard invariant set has a singularity (e.g., a tangent periodic orbit or a corner polygon). Then, under some conditions on the potential and the geometry [14,16], a stability wedge in the $(\mu,\varepsilon)$ plane emanates from $(\mu^*,0)$, i.e., the smooth flow has stable periodic orbit for all parameters in this wedge. For a

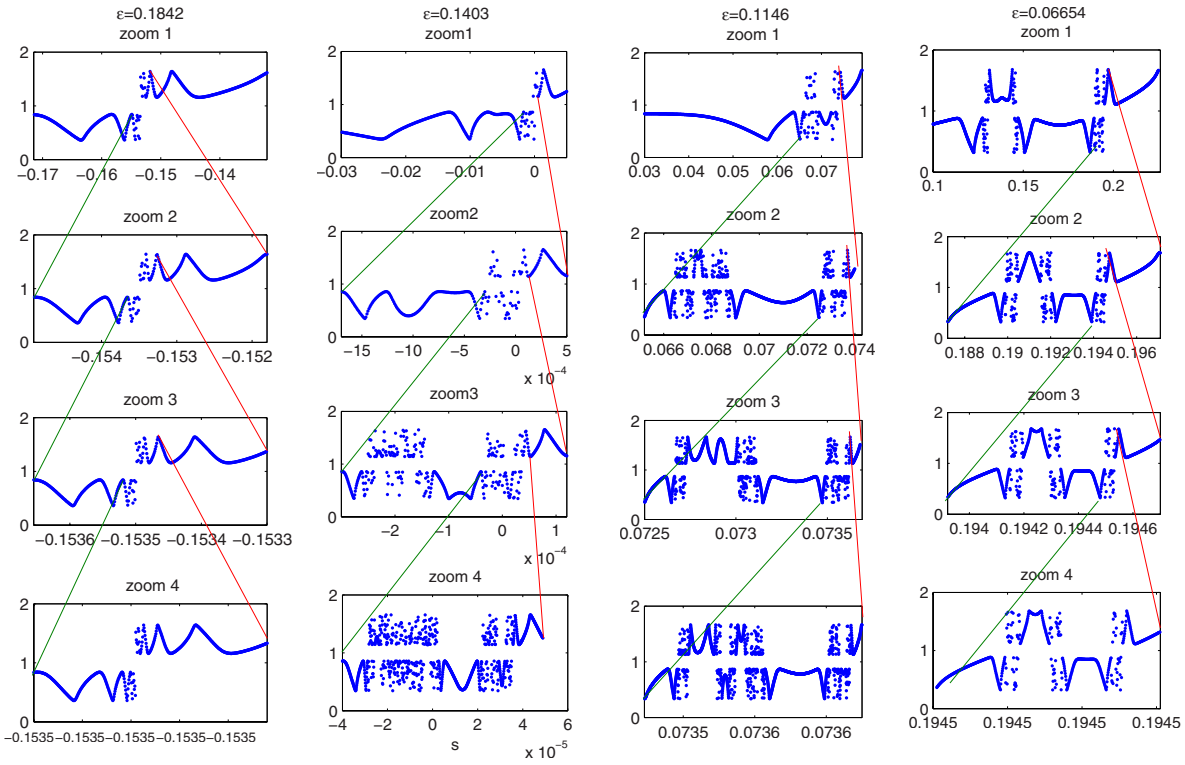


FIG. 10. (Color online) Self-similar (outer columns) and singular (middle columns) scattering functions: closeups of unresolved regions of the scattering function $\Phi_2(s;\epsilon)$ for $\epsilon$=0.1842, 0.1403, 0.1146, and 0.066 54 are shown.

fixed $\mu$ value intersecting this wedge, there exist an interval of $\varepsilon$ values, $[\varepsilon^-(\mu),\varepsilon^+(\mu)]$, at which the periodic orbit is stable. Fixing such a "generic" $\mu$ value close to $\mu^*$, where at $\mu$ the billiard invariant set is hyperbolic and nonsingular and $\varepsilon^{\pm}(\mu)$ are small, the following sequence of bifurcations occurs as $\varepsilon$ is increased from $0^+$:

(1) For a sufficiently small $\varepsilon$ the hyperbolicity is preserved so the scattering function is self-similar, and its fractal dimension approaches that of the billiard scattering function at $\mu$. Isolated discontinuities in the billiard scattering function may lead to additional singular components in the scattering function of the smooth flow.

(2) Increasing $\varepsilon$ towards and through the interval $[\varepsilon^-(\mu),\varepsilon^+(\mu)]$ leads to a sequence of Hamiltonian bifurcations of the hyperbolic periodic orbits that produces elliptic orbits. These bifurcations appear in the scattering function as the merge between several unresolved regions. For $\varepsilon$ values inside the wedges of stability, the signature of nonhyperbolic chaotic scattering shows up—the density of singularities is large and does not appear to converge to a discrete set as further magnifications are employed. We notice that the stability interval $[\varepsilon^-(\mu),\varepsilon^+(\mu)]$ indicates the stability property of a single periodic orbit. At least near the period-doubling end of this interval there exist a cascade of other periodic orbits that are stable, hence, the nonhyperbolic interval is certainly larger than $[\varepsilon^-(\mu),\varepsilon^+(\mu)]$.

(3) Further small increase of $\varepsilon$ beyond the stability interval may lead to the appearance of an additional interval of hyperbolic scattering or to the appearance of another interval of stability that stems from another stability wedge emanating from some other $\mu^{**}$. Depending on how far the stability wedges are located from each other, the scattering may be either nonhyperbolic (with some KAM tori) or hyperbolic with a fractal dimension that is smaller than the one appearing for the billiard limit.

(4) A larger increase in $\varepsilon$ is problem specific and may involve some topological changes of the corresponding Hill's region. In our examples, it finally leads to the reduction of the invariant set to one unstable periodic orbit and then to the destruction of the invariant set.

The above description suggests that by choosing a one parameter family of steep potentials $(\mu,\varepsilon(\mu))\to(\mu^*,0)$ such that $\varepsilon(\mu)\in(\varepsilon^-(\mu),\varepsilon^+(\mu))$ for all $\mu$ values (see Fig. 6), the fractal dimension of the corresponding scattering function is close to two for arbitrary small $\varepsilon$. On the other hand, we have seen that for a fixed $\mu\neq\mu^*$, for sufficiently small $\varepsilon$, hyperbolic chaotic scattering is observed. Thus, we propose that near $\mu^*$ the fractal dimension of the scattering function can be controlled by varying $\varepsilon/(\mu-\mu^*)$.

From a mathematical point of view, Theorem 1 shows that classes of smooth Hamiltonian systems having hyperbolic repellors that can be fully characterized by symbolic dynamics may be easily found: these are systems with steep potentials that limit to regular Sinai scatterer—such scatterers have nonsingular hyperbolic repellors (i.e., all orbits of the repellors are bounded away from being tangent and from the corners). In this case the scattering properties of the steep smooth flows and of the limiting billiards are similar and robust: we expect the fractal dimension of the scattering function of the smooth flow to limit to that of the billiard and to change continuously with small smooth deformation of the billiard's geometry. Examples of such systems had pre-

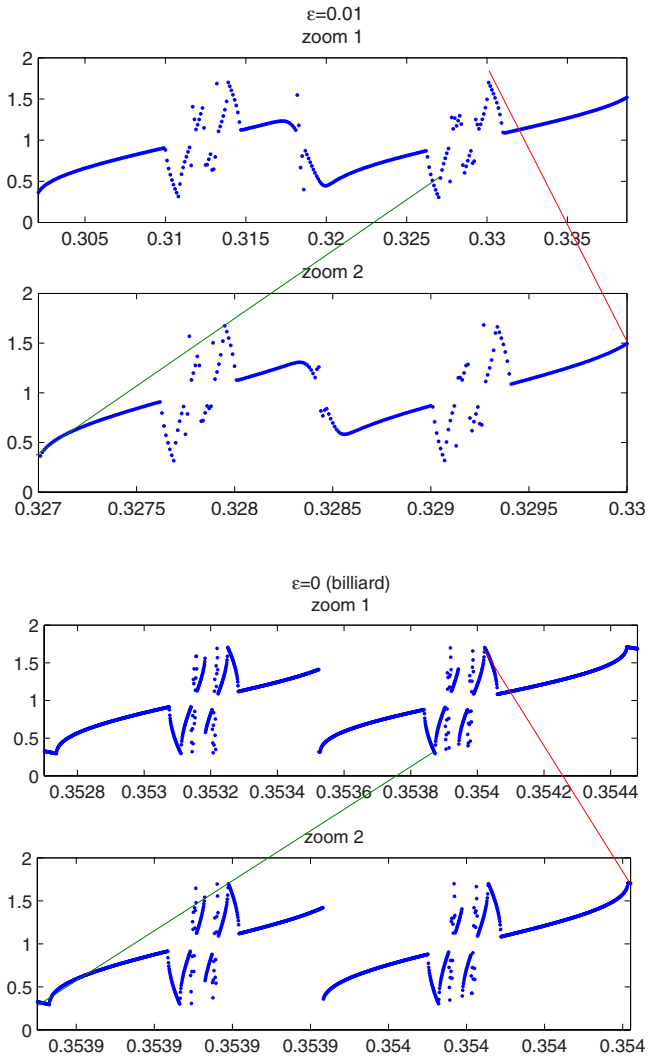


FIG. 11. (Color online) Similarity between the scattering functions of the smooth flow and the billiard: closeup of unresolved regions of $\Phi_2(s;\epsilon)$ for $\epsilon=0.01$ and the billiard limit are shown.

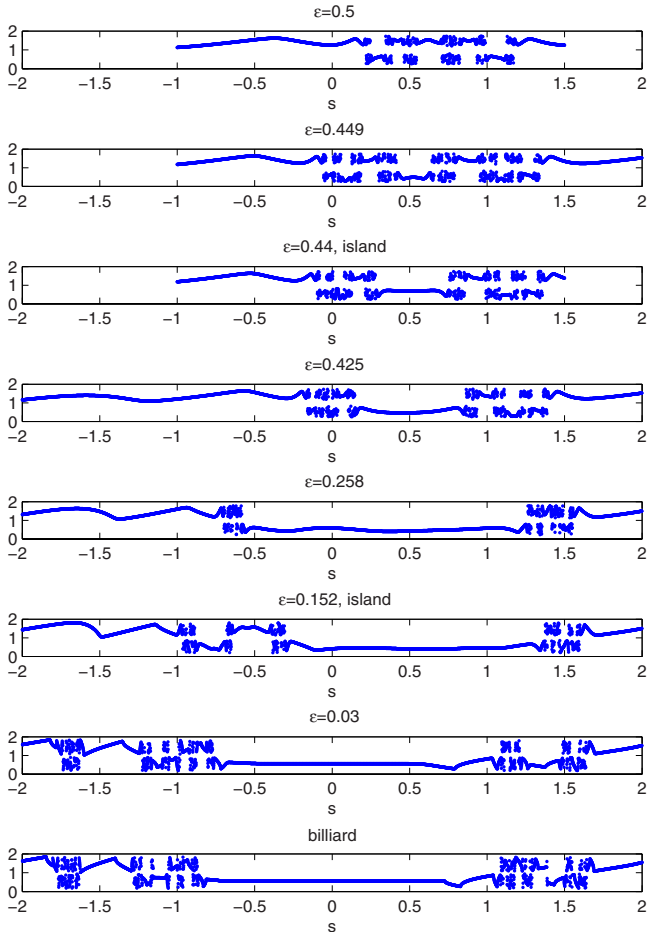


FIG. 12. (Color online) Scattering function $\Phi(s;\epsilon)$ for the tangent case at $\mu=0.1$.

viously appeared as prototypes for demonstrating hyperbolic chaotic scattering, yet, utilizing the billiard limit allows one to rigorously establish such results in their full generality (without assuming specific geometry and for a large class of potentials). Moreover, our approach suggests when the repellors are expected to change their hyperbolic character due to geometrical effects—exactly when singularities are encountered (low-energy effects, such as the abrupt bifurcation disappear in our setting in the limit $\varepsilon\to 0$).

Indeed, the framework of studying scattering by steep potentials leads naturally to the exploration of billiard singularities. In the two-dimensional case, this approach led us to study corners; we observed two new mechanisms to increase the complexity of the billiards scattering function—one by increasing the number of corners and the other by making some of the corners sharper. These preliminary observations suggest that one should study in more detail the signature of different types of corners on the billiard scattering function and on the corresponding scattering by steep smooth potentials. Moreover, studying the role of singularities in higher dimensional billiard scatterers and their smooth counterpart is an exciting natural extension of this approach (e.g., the corner singularity may create islands of effective stability in the corresponding smooth Hamiltonians in arbitrarily high dimensions [13]).

## ACKNOWLEDGMENTS

We thank Uzy Smilansky and Dmitry Turaev for stimulating discussions and important comments. We acknowledge support by the Israel Science Foundation (Grant No. 926/04), and by a joint grant from the Ministry of Science, Culture and Sport, Israel and the Russian Foundation for Basic Research, the Russian Federation (MNTI-RFBR grant No. 06-01-72023).

## APPENDIX: CLOSENESS THEORY

Let us first recall the conditions $W(q;\varepsilon)$ needs to satisfy so that the regular trajectories of a billiard will be shadowed by trajectories of the smooth flow ([12] applied to $\mathcal{D}=S^{\text{interior}}_{\bar{R}+\Delta}\backslash D$ for some $\Delta>0$).

*Condition I.* For any fixed (independent of $\varepsilon$) $\bar{R}$ and a compact region $K\subset\mathcal{D}$ the potential $W(q;\varepsilon)$ diminishes along with all its derivatives as $\varepsilon\to 0$ as follows:

$$\lim_{\varepsilon\to 0}\| W(q;\varepsilon)|_{q\in K}\|_{C^{r+1}} = 0. \tag{A1}$$

The growth of the potential near the boundary for sufficiently small $\varepsilon$ values is treated as in [14]. We assume that the level sets of $W$ may be realized by some *finite* function near the boundary. Namely, let $N(\Gamma^*)$ denote the fixed (independent of $\varepsilon$) neighborhood of the corner set and $N(\Gamma_i)$ denote the fixed neighborhood of the smooth boundary component $\Gamma_i$; define $\tilde{N}_i = N(\Gamma_i)\backslash N(\Gamma^*)$ (we assume that $\tilde{N}_i \cap \tilde{N}_j = \emptyset$ when $i \neq j$). Assume that for all small $\varepsilon \geq 0$ there exists *a pattern function*

$$Q(q;\varepsilon): \cup_i \tilde{N}_i \to \mathbb{R}^1,$$

which is $C^{r+1}$ with respect to $q$ in each of the neighborhoods $\tilde{N}_i$ and it depends continuously on $\varepsilon$ (in the $C^{r+1}$ topology, so it has, along with all derivatives, a proper limit as $\varepsilon \to 0$). Further assume that in each of the neighborhoods $\tilde{N}_i$ the following is fulfilled.

*Condition II(a).* The billiard boundary is composed of level surfaces of $Q(q;0)$ as follows:

$$Q(q;\varepsilon = 0)\big|_{q\in\Gamma_i\cap\tilde{N}_i} \equiv Q_i = \text{constant}. \tag{A2}$$

In the neighborhood $\tilde{N}_i$ of the boundary component $\Gamma_i$ [so $Q(q;\varepsilon)$ is close to $Q_i$], define *a barrier function* $\mathcal{W}_i(Q;\varepsilon)$, which is $C^{r+1}$ in $Q$, continuous in $\varepsilon$ and does not depend explicitly on $q$, and assume that there exists $\varepsilon_0$ such that

*Condition II(b).* For all $\varepsilon \in (0,\varepsilon_0]$ the potential level sets in $\tilde{N}_i$ are identical to the pattern function level sets and thus

$$W(q;\varepsilon)\big|_{q\in\tilde{N}_i} \equiv \mathcal{W}_i(Q(q;\varepsilon) - Q_i;\varepsilon), \tag{A3}$$

and

*Condition II(c).* For all $\varepsilon \in (0,\varepsilon_0]$, $\nabla W$ does not vanish in the finite neighborhoods of the boundary surfaces, $\tilde{N}_i$, thus

$$\nabla Q\big|_{q\in\tilde{N}_i} \neq 0, \tag{A4}$$

and for all $Q(q;\varepsilon)|_{q\in\tilde{N}_i}$,

$$\frac{d}{dQ}\mathcal{W}_i(Q - Q_i;\varepsilon) \neq 0. \tag{A5}$$

Now, the rapid growth of the potential across the boundary may be described in terms of the barrier functions alone. Note that by Eq. (A4), the pattern function $Q$ is monotone across $\Gamma_i \cap \tilde{N}_i$, so either $Q > Q_i$ corresponds to the points near $\Gamma_i$ inside $K$ and $Q < Q_i$ corresponds to the outside, or vice versa. To fix the notation, we will adopt the first convention.

*Condition III.* There exists a constant (may be infinite) $\mathcal{E}_i > 0$ such that as $\varepsilon \to +0$ the barrier function increases from zero to $\mathcal{E}_i$ across the boundary $\Gamma_i$ as follows:

$$\lim_{\varepsilon\to+0} \mathcal{W}(Q;\varepsilon) = \begin{cases} 0, & Q > Q_i \\ \mathcal{E}_i, & Q = Q_i \end{cases}. \tag{A6}$$

Let

$$\mathcal{E} = \min_{i=1,\ldots,\bar{n}} \mathcal{E}_i. \tag{A7}$$

By Eq. (A5), for small $\varepsilon$, $Q$ could be considered as a function of $\mathcal{W}$ and $\varepsilon$ near the boundary: $Q = Q_i + \mathcal{Q}_i(\mathcal{W};\varepsilon)$. Condition IV states that for small $\varepsilon$ a finite change in $\mathcal{W}$ corresponds to a small change in $Q$:

*Condition IV.* As $\varepsilon \to +0$, for any fixed $\mathcal{W}_1$ and $\mathcal{W}_2$ such that $0 < \mathcal{W}_1 < \mathcal{W}_2 < \mathcal{E}$, for each boundary component $\Gamma_i$, the function $\mathcal{Q}_i(\mathcal{W};\varepsilon)$ tends to zero uniformly on the interval $[\mathcal{W}_1, \mathcal{W}_2]$ along with all its $(r+1)$ derivatives.

In [12] it was shown that not only can we establish that the regular hyperbolic orbits of the billiard flow and the smooth flow are close, we can even find the order of the correction terms. To obtain these error estimates, near each boundary component $\Gamma_i$, two boundary layers of width $\eta_i(\varepsilon) \leq \delta(\varepsilon)$ are defined. The thicker boundary layer is chosen so that $W(q;\varepsilon)$ and its $r+1$ derivatives are smaller than $m^{(r)}(\delta;\varepsilon)$ in $\mathcal{D}^\varepsilon_{\text{int}}$—the region $\mathcal{D}$ stripped of the boundary layers of width $\delta(\varepsilon)$ and some fixed regions near the corner set. The thinner boundary layer is chosen so that $\mathcal{Q}(\mathcal{W})$ and its $r+1$ derivatives are smaller than $M_i^{(r)}(\nu_i;\varepsilon)$ in it, where $\nu_i = \mathcal{W}[Q_i + \eta_i(\varepsilon)]$ (so the thin boundary layer has the potential level sets in the range $[\nu_i, h]$). $\mathcal{D}^\varepsilon$, the auxiliary billiard region, is defined to be $\mathcal{D}$ stripped of the thin boundary layers of widths $\eta_i(\varepsilon)$ and some fixed regions near the corner set. Table 3.3.1 in [12] summarizes the optimized choice of $\eta(\varepsilon)$, $\delta(\varepsilon)$, $m^{(r)}(\delta;\varepsilon)$, $M^{(r)}(\nu_i;\varepsilon)$ so that the difference between the trajectories of the smooth flow and of the billiard flow in $\mathcal{D}^\varepsilon$ is smallest in the $C^r$ norm for some typical potentials. For example, for the exponential potential, a boundary layer width of order $O(\varepsilon|\ln\varepsilon|)$ may be chosen so that the auxiliary billiard regular trajectories are $O_{C^r}(\sqrt[r+2]{\varepsilon})$ close to the corresponding smooth flow trajectories. Moreover, for regular reflections a Poincaré map $\Phi^\varepsilon$ of the smooth flow is defined by the cross section

$$S_\varepsilon = \{\rho = (q,p):\ q \in \partial D^\varepsilon,\ \langle p, n(q)\rangle > 0\}, \tag{A8}$$

and for regular orbits—orbits that intersect $\partial D^\varepsilon$ at an angle bounded away from zero, this map is $C^r$ close to the auxiliary billiard map $B^\varepsilon$ in $\mathcal{D}^\varepsilon$. As the billiard map $B^\varepsilon$ is close to the original billiard map $B$, we obtain the closeness of the Poincaré map $\Phi^\varepsilon$ to $B$ as well (the map $B^\varepsilon$, rather than $B$, is used as the zeroth-order approximation for an explicit asymptotic expansion for $\Phi^\varepsilon$). Taking a fixed $\Delta > 0$ so that the section $q \in S_R^-$ consists of interior points of the billiard flow in $\mathcal{D}$, we combine these results of [12] and the formulation of Sec. II to establish the following theorem:

*Theorem 3.* Consider a Hamiltonian system with a potential $W(q,\varepsilon)$ satisfying Conditions I–IV in the domain $\mathcal{D} = S^{\text{interior}}_{R+\Delta}\backslash D$, where $D$ is a Sinai scatterer and $\Delta > 0$. Choose $\nu(\varepsilon), \delta(\varepsilon)$, and $r \geq 1$ such that $\nu(\varepsilon), \delta(\varepsilon), m^{(r)}(\varepsilon), M^{(r)}(\varepsilon) \to 0$ as $\varepsilon \to 0$. Let $P^b(t)$ denote a regular hyperbolic orbit for the billiard flow in $\mathcal{D}$. Then, for any $h \in (0,\mathcal{E})$, for sufficiently small $\varepsilon$, the smooth Hamiltonian flow has a uniquely defined hyperbolic orbit $P^\varepsilon(t)$ which stays $O_{C^r}(\nu + m^{(r)} + M^{(r)})$ close to $P^b(t)$ for all $t$ outside of the collision intervals (finitely many of them in any finite interval of

time) of length $O(|\delta|+M^{(r)})$. Away from the collision intervals, the local Poincaré map near $P^\varepsilon$ is $O_{C^r}(\nu+m^{(r)}+M^{(r)})$ close to the local Poincaré map near $P^b(t)$. Moreover, for all hyperbolic orbits, the stable and unstable manifolds of $P^\varepsilon$ approximate $O_{C^r}(\nu+m^{(r)}+M^{(r)})$ closely the stable and unstable manifolds of $P^b(t)$ on any compact, forward-invariant or, respectively, backward-invariant piece bounded away from the singularity set in the billiard's phase space.

*Proof.* See Theorem 5 of [12] where this theorem is proved for periodic orbits. Here we simply use the note of [12] that the same results and proof apply to any regular hyperbolic orbit, with the same error estimates as for the hyperbolic periodic orbit case (by regular hyperbolic orbit, we mean that this orbit is bounded away from the singularity set). ■

Using the existence of a Poincaré map $\Phi^\varepsilon$ that is close to the billiard map away from tangent reflections, it is easy to establish that regular hyperbolic sets appear also for the smooth flow as stated in Theorem 1. Indeed, consider the billiard partition which is used to construct $\Lambda$. By assumption on the regularity of $D$, each component is mapped to its image by a regular reflection (namely, there are no tangent reflections). It follows that for sufficiently small $\varepsilon$, the image of the partition components under the Poincaré map $\Phi^\varepsilon$, which is well defined for all orbits in these components since they all have nontangent reflections, is close, in the $C^r$ topology, to the image of the components under the auxiliary billiard map (i.e., both the topology of the invariant set and the hyperbolicty properties that are governed by the first derivatives of the billiard map are inherited by the Poincaré map of the smooth flow). It follows that the invariant sets of $\Lambda$ and $\Lambda^\varepsilon$ are conjugated by the same symbolic dynamics and that their Lyapunov exponents and cone structure are $C^r$ close as well. Similar arguments hold for the more general setting as long as the hyperbolic invariant set of the billiard is regular and isolated from all singularities. Let us now examine how these results translate to the properties of the scattering map.

*Corollary 1.* Under the same conditions of Theorem 3, if $(s_{\text{in}}(b_{\text{in}},\varphi_{\text{in}};\bar{R}),\varphi_{\text{in}})$ is a nontrivial regular value [respectively, $(s_{\text{in}},\varphi_{\text{in}})\in\Sigma_{\tan}$ has a finite number of collisions, one tangent and all the rest regular] of the billiard scattering map $S$, then there exists a nearby initial condition $(s^\varepsilon_{\text{in}},\varphi^\varepsilon_{\text{in}})$, limiting to $(s_{\text{in}},\varphi_{\text{in}})$ as $\varepsilon\to 0$, such that the smooth scattering map $S^\varepsilon$ is $C^r$ close (respectively, is $C^0$ close) to $S$ at $(s_{\text{in}},\varphi_{\text{in}})$. Furthermore, for the regular case, away from the short collision intervals of length $O(|\delta|+M^{(1)})$, the orbit of $(s^\varepsilon_{\text{in}},\varphi^\varepsilon_{\text{in}})$ is $O(\nu+m^{(1)}+M^{(1)})$-close to the corresponding orbit of the billiard flow.

*Proof.* Note that $S(\bar{R})$ is, by its definition in Sec. II, a local Poincaré map near a regular hyperblic orbit, and, since $\Delta>0$ it corresponds to a legitimate Poincaré section inside $\mathcal{D}$ and bounded away from the collision intervals. Recall that the scatterers are assumed to be dispersing so if $(s_{\text{in}},\phi_{\text{in}})$ is a regular orbit it is necessarily hyperbolic. Hence the results for a nontrivial regular value follow from theorem 3. The results regarding the tangent orbit follow from the same construction, and, from the proof in [12,14] regarding the $C^0$ closeness of the billiard map and the smooth flow near tangent collisions. ■

Taking only two circular obstacles, as in the first example of [47], supplies a clear demonstration of these persistent results in the simple nonchaotic setting (not shown for bravity). Figures 12 and 3 demonstrate these closeness results in the chaotic case for sufficiently small $\varepsilon$ (nonuniformly in the distance from the singular Sinai scatterers).

Finally, we note that we did not analyze the far field behavior of the scattering functions, behavior which depends on the rate of decay of the potential. In principle, to obtain similar results uniformly in $\bar{R}$, so that impact coordinates may be used in the smooth case, one needs to impose sufficiently rapid decay rate of the potential at large $q$ values. We propose that imposing the following condition should suffice:

*Condition V.* There exists an $\bar{R}$, such that for all $|q|\geq\bar{R}$, there exists $\alpha>0$ ($\bar{R}$ and $\alpha$ are independent of $\varepsilon$) and a function $A(\varepsilon)$ which limits to 0 as $\varepsilon\to 0$, such that for all $\varepsilon\in(0,\varepsilon_{\max})$

$$|W(q;\varepsilon)|\leq\frac{A(\varepsilon)}{|q|^\alpha}, \tag{A9}$$

in the $C^{r+1}$ topology.

Indeed, using this condition, it can be shown, by successive approximation method of the integral form of the Hamiltonian flow (2), that the asymptotic velocities $(p^\varepsilon_x(\pm\infty),p^\varepsilon_y(\pm\infty))$ and thus the corresponding asymptotic directions $\varphi^\varepsilon_{\text{in,out}}$ may be defined on $S_{\bar{R}}$ (see, e.g. [16] for a similar construction near corners). While Eq. (A9) is not sufficient to guarantee that an asymptotic direction $s_{\text{in}}$ exists, it is still possible to define asymptotic impact parameter $\eta_{\text{in}}$ as in [16]. Then the mapping from $S(R_\infty)$ where $R_\infty\gg R$ to $S(\bar{R})$ is smooth and the properties of the smooth scattering map at $S(\bar{R})$ are inherited by the smooth scattering map at $S(R_\infty)$.


[1] The behavior of a point particle traveling with a constant speed in a region $\mathcal{D}\subset R^N$, undergoing elastic collisions at the regions's boundary, is known as the billiard problem.

[2] M. Gutzwiller, *Chaos in Classical and Quantum Mechanic* (Springer-Verlag, New York, 1990).

[3] U. Smilansky, in *Semiclassical Quantization of Chaotic Billiards—A Scattering Approach*, Proceedings of the 1994 Les-Houches summer school on, "Mesoscopic Quantum Physics," edited by A. Akkermans, G. Montambaux, and J. Pichard (Elsevier, 1995).

[4] D. Szász, Stud. Sci. Math. Hung. **31**, 299 (1996).

[5] P. Gaspard and S. Rice, J. Chem. Phys. **90**, 2225 (1989).

[6] Y.-C. Chen, Dyn. Syst. **19**, 145 (2004).

[7] M. Klein and A. Knauf, *Classical Planar Scattering by Cou-*

*lombic Potentials* (Springer-Verlag, New York, 1992).
[8] A. Knauf, J. Eur. Math. Soc. **4**, 1 (2002).
[9] A. Kaplan, N. Friedman, M. Andersen, and N. Davidson, Phys. Rev. Lett. **87**, 274101 (2001).
[10] Y.-H. Kim, U. Kuhl, H.-J. Stockmann, and J. P. Bird, J. Phys.: Condens. Matter **17**, L191 (2005).
[11] A. Rapoport and V. Rom-Kedar, Chaos **16**, 043108 (2006).
[12] A. Rapoport, V. Rom-Kedar, and D. Turaev, Commun. Math. Phys. **272**, 567 (2007).
[13] A. Rapoport, V. Rom-Kedar, and D. Turaev, Commun. Math. Phys. (to be published).
[14] V. Rom-Kedar and D. Turaev, Physica D **130**, 187 (1999).
[15] D. Turaev and V. Rom-Kedar, Nonlinearity **11**, 575 (1998).
[16] D. Turaev and V. Rom-Kedar, J. Stat. Phys. **112**, 765 (2003).
[17] E. Ott and T. Tel, Chaos **3**, 417 (1993).
[18] E. Ott, *Chaos in Dynamical Systems*, 2nd ed. (Cambridge University Press, Cambridge, England, 2002).
[19] L. Benet, T. Seligman, and D. Trautmann, Celest. Mech. Dyn. Astron. **71**, 167 (1998).
[20] P. T. Boyd and S. L. W. McMillan, Chaos **3**, 507 (1993).
[21] J. Hietarinta and S. Mikkola, Chaos **3**, 183 (1993).
[22] O. Merlo and L. Benet, Celest. Mech. Dyn. Astron. **97**, 49 (2007).
[23] J. Moser and P. J. Holmes, *Stable and Random Motions in Dynamical Systems: With Special Emphasis on Celestial Mechanics* (Princeton University Press, Princeton, NJ, 2001).
[24] J.-M. Petit and M. Henon, Astron. Astrophys. **188**, 198 (1987).
[25] W. Breymann, Z. Kovács, and T. Tél, Phys. Rev. E **50**, 1994 (1994).
[26] A. A. Chernikov and G. Schmidt, Chaos **3**, 525 (1993).
[27] H. Aref, J. Fluid Mech. **192**, 115 (1984).
[28] C. Jung, T. Tel, and E. Ziemniak, Chaos **3**, 555 (1993).
[29] C. Jung and E. Ziemniak, J. Phys. A **25**, 3929 (1992).
[30] E. A. Novikov and I. B. Sedov, Zh. Eksp. Teor. Fiz. **77**, 588 (1979).
[31] V. Rom-Kedar, A. Leonard, and S. Wiggins, J. Fluid Mech. **214**, 347 (1990).
[32] B.-P. Koch and B. Bruhn, Chaos **3**, 443 (1993).
[33] D. W. Noid, S. K. Gray, and S. A. Rice, J. Chem. Phys. **84**, 2649 (1986).
[34] C. C. Rankin and W. H. Miller, J. Chem. Phys. **55**, 3150 (1971).
[35] D. Wintgen, K. Richter, and G. Tanner, Chaos **2**, 19–33 (1992).
[36] J.-M. Yuan and Y. Gu, Chaos **3**, 569 (1993).
[37] B. Eckhardt, J. Phys. A **20**, 5971 (1987).
[38] C. Jung and H. J. Scholz, J. Phys. A **20**, 3607 (1987).
[39] Usually one uses the box-counting or the uncertainty dimension [45,46,57]. The singularity set along a ray corresponds to the set at which the scattering function is singular so its dimension is $d_\Phi - 1$.
[40] See, however, [74,75], where it was shown that a regular invariant set can produce a fractal scattering function as well. As explained in [74,75], the constructed counterexamples are nongeneric (e.g., [75] uses a potential having extrema on a Cantor set for arbitrary high energies—such a potential is excluded here by condition II(c) in the Appendix. Reference [74] uses a nongeneric geometrical setting).
[41] S. Bleher, C. Grebogi, E. Ott, and R. Brown, Phys. Rev. A **38**, 930 (1988).
[42] S. Ree and L. E. Reichl, Phys. Rev. E **65**, 055205(R) (2002).
[43] M. Hénon, Physica D **33**, 132 (1988).
[44] J. R. Dorfman and P. Gaspard, Phys. Rev. E **51**, 28 (1995).
[45] S. Bleher, C. Grebogi, and E. Ott, Physica D **46**, 87 (1990).
[46] S. Bleher, E. Ott, and C. Grebogi, Phys. Rev. Lett. **63**, 919 (1989).
[47] M. Ding, C. Grebogi, E. Ott, and J. A. Yorke, Phys. Rev. A **42**, 7025 (1990).
[48] K. T. Hansen and A. Kohler, Phys. Rev. E **54**, 6214 (1996).
[49] A. Knauf and I. Taimanov, Math. Ann. **331**, 631 (2005).
[50] G. Troll and U. Smilansky, Physica D **35**, 34 (1989).
[51] References [7,8,49] considered also attractive Coulombic potentials—for this part of their work our results do not apply.
[52] V. Daniels, M. Vallieres, and J.-M. Yuan, Chaos **3**, 475 (1993).
[53] V. J. Daniels, M. Vallieres, and J.-M. Yuan, Phys. Rev. E **57**, 1519 (1998).
[54] C. F. Hillermeier, R. Bl"umel, and U. Smilansky, Phys. Rev. A **45**, 3486 (1992).
[55] Y. Lau, J. Finn, and E. Ott, Phys. Rev. Lett. **66**, 978 (1991).
[56] K. R. Meyer and R. G. Hall, *Introduction to Hamiltonian Dynamical Systems and the N-Body Problem*, Applied Mathematical Sciences, Vol. 90 (Springer-Verlag, New York, 1991).
[57] At $E_c$, the energy surface contains a saddle point and its separatrices, so this bifurcation may be related to the study of homoclinic bifurcations [76,77].
[58] T. Tel, C. Grebogi, and E. Ott, Chaos **3**, 495 (1993).
[59] E.g., to study scattering by Lennard-Jones potentials at high energies, set $\varepsilon = 1/h$, and rescale $H$ and $p$ by $h$ and $\sqrt{h}$, respectively.
[60] Dispersing geometries with cusps are not Sinai scatterers.
[61] P. Gaspard, *Chaos, Scattering and Statistical Mechanics* (Cambridge University Press, Cambridge, England, 1998).
[62] If the trajectory of $(b_{\text{in}}, \varphi_{\text{in}})$ does not hit the scatterer it is called trivial and $J(b_{\text{in}}, \varphi_{\text{in}})$ is defined to be the empty set.
[63] For $n$ disjoint scatterers, $\chi$ is a vector of $n$ circles and a counter which points to the current component.
[64] For other scatterers, in addition to the possible appearance of nonhyperbolic invariant set, the transient behavior near focusing components (having whispering orbits), cusps, and deflection points needs to be analyzed.
[65] Y. Sinai, Russ. Math. Surveys **25**, 137 (1970).
[66] The (nongeneric) intersection of $p+2$ such lines corresponds to orbits with $p+2$ tangencies and is expected to appear with $p > 0$ only in nongeneric cases: symmetric cases or higher codimension settings in which $p$-parameter families of scatterers are considered.
[67] In a family of segments, there may also appear some isolated $(b_{\text{in}}, \varphi_{\text{in}})$ values at which two of the singularity lines and $\mathcal{T}(b_{\text{in}}, \varphi_{\text{in}})$ cross, namely, a triple intersection appears.
[68] The angle between the tangent lines at the point of the intersection of the circles.
[69] By $O_{C^{r+1}}(\frac{1}{z^\alpha})$ we mean that the $r$ derivatives of $V$ decay at least as fast as the corresponding $r+1$ derivatives of $\frac{1}{z^\alpha}$.
[70] The auxiliary billiard, defined in [12] (see also the ), may be a useful concept for such $\varepsilon$ values.
[71] The relation to the Poincaré scattering map, defined in analogy to the quantum $S$ matrix (see [78]), may be found, provided the potential decays sufficiently rapidly away from the scatterers, by using the impact coordinates.
[72] Namely, for small $(s, \varphi)$, for sufficiently small $\varepsilon$, $S^\varepsilon(s^\varepsilon_{\text{in}}$

$+s, \varphi_{\text{in}}^{e}+\varphi)-S(s_{\text{in}}+s, \varphi_{\text{in}}+\varphi)$ and the $r$ derivatives of this map with respect to $(s, \varphi)$ are small.

[73] demonstrating that orbits escape from this region at an exponential rate may have been more convincing. Indeed, the dependence of the escape rates on $\mu$ in the billiard case and on $(\mu, \epsilon)$ in the smooth case is interesting and needs to be further studied.

[74] C. Jung, C. Mejia-Monasterio, and T. H. Seligman, Phys. Lett. A **198**, 306 (1995).

[75] G. Troll, Chaos, Solitons Fractals, **7**, 1929 (1996).

[76] L. P. Shilnikov and D. V. Turaev, Regular Chaotic Dyn. **2**, 126 (1997) [V. I. Arnold (on the occasion of his 60th birthday)] (Russian).

[77] D. V. Turaev and L. P. Shilnikov, Dokl. Akad. Nauk SSSR **304**, 811 (1989).

[78] C. Jung and T. H. Seligman, Phys. Rep. **285**, 77 (1997).